# SCIENTIFIC REP🝆RTS

**OPEN**

# Fragment-based screening identifies inhibitors of ATPase activity and of hexamer formation of Cagα from the *Helicobacter pylori* type IV secretion system

Tarun Arya, Flore Oudouhou, Bastien Casu, Benoit Bessette, Jurgen Sygusch & Christian Baron (ORCID)

Type IV secretion systems are multiprotein complexes that mediate the translocation of macromolecules across the bacterial cell envelope. In *Helicobacter pylori* a type IV secretion system encoded by the *cag* pathogenicity island encodes 27 proteins and most are essential for virulence. We here present the identification and characterization of inhibitors of Cagα, a hexameric ATPase and member of the family of VirB11-like proteins that is essential for translocation of the CagA cytotoxin into mammalian cells. We conducted fragment-based screening using a differential scanning fluorimetry assay and identified 16 molecules that stabilize the protein suggesting that they bind Cagα. Several molecules affect binding of ADP and four of them inhibit the ATPase activity. Analysis of enzyme kinetics suggests that their mode of action is non-competitive, suggesting that they do not bind to the active site. Cross-linking suggests that the active molecules change protein conformation and gel filtration and transmission electron microscopy show that molecule 1G2 dissociates the Cagα hexamer. Addition of the molecule 1G2 inhibits the induction of interleukin-8 production in gastric cancer cells after co-incubation with *H. pylori* suggesting that it inhibits Cagα *in vivo*. Our results reveal a novel mechanism for the inhibition of the ATPase activity of VirB11-like proteins.

*Helicobacter pylori* is a widespread pathogenic bacterium that lives in the stomach of over half of the world's population[1]. The infection with virulent strains causes inflammatory reactions, gastritis, peptic ulcers and it is one of the principal causes of stomach cancer in humans[2,3]. Antibiotic treatments using combination therapies of three or four drugs have generally been successful, but eradication therapy is becoming increasingly difficult due to rising resistance against many antimicrobial agents, such as clarithromycin and metronidazole[4]. Novel treatment options are therefore urgently needed and targeting bacterial virulence factors to attenuate the inflammation is a strategy that could complement or even replace currently used eradication treatments.

Type IV secretion systems (T4SS) mediate the transfer of virulence factors across the cell envelope of many bacterial pathogens as well as the exchange of plasmids contributing to the spread of antibiotic resistance genes[5,6]. *H. pylori* strains encode T4SSs that mediate the uptake of DNA as well as bacterial virulence like the *cag* pathogenicity island (*cag*-PAI)-encoded T4SS; this system comprises 27 components of which most are essential for bacterial virulence[7–10]. The *cag*-PAI is required for the transfer of the CagA cytotoxin into mammalian cells where it is phosphorylated by Src kinase at tyrosine residues and its interactions with mammalian proteins such as SHP-2 and Grb-2 lead to rearrangements of the cytoskeleton and to proinflammatory reactions[11]. The *cag*-PAI-encoded T4SS is also a conduit for bacterial murein and for the small molecule metabolite heptulose-1,7-bisphosphate triggering signalling cascades via Nod-1 and TIFA, respectively, that contribute to the proinflammatory response[12,13].

The *H. pylori* cag-PAI encodes 27 proteins including homologs of all 12 components of the most studied model T4SS from *Agrobacterium tumefaciens*[9]. These conserved proteins are critical for secretion system function and they are either part of surface-exposed pili of the periplasmic T4SS core complex or they energize T4SS assembly

Department of Biochemistry and Molecular Medicine, Faculty of Medicine, Université de Montréal, Québec, Canada. Correspondence and requests for materials should be addressed to C.B. (email: christian.baron@umontreal.ca)

or substrate translocation. We here focus on the Cagα (HP0525) protein that is a member of the VirB11 family of ATPases present in all T4SSs. Electron microscopic (EM) analyses and X-ray crystallography have shown that the overall structures of VirB11-like proteins from different organisms are very similar comprising homo-hexameric rings[14,15]. The monomeric subunit consists of an N-terminal domain (NTD) and a C-terminal domain (CTD) that are linked via a short linker region comprising the nucleotide binding site. The X-ray structures of Cagα apoprotein[16], as well as of its complexes with ADP[17] and with the inhibitor ATPγS[16] have been solved. These studies revealed that the CTD forms a 'six clawed grapple' mounted onto the NTD, forming a hexameric ring and a dome-like chamber that is closed at one end and opened at the other[17]. Glycerol gradient centrifugation showed a large conformational change of VirB11 homologs from plasmid RP4 (TrbB) and *H. pylori* upon binding to ATP, underlining the dynamic nature of the protein[16,18]. The other available X-ray structure from *Brucella suis* VirB11 differs from Cagα by a domain swap of the large linker region between NTD and CTD[19], but the overall structure is very similar.

Since T4SS are important for bacterial virulence they are very interesting targets for the development of drugs that disarm but do not kill bacterial pathogens[20,21]. In our previous work, we have identified inhibitors of the dimerization of VirB8-like proteins from *B. suis* and plasmid pKM101 using the bacterial two-hybrid system and fragment-based screening approaches and we identified molecules that reduce T4SS function[22–25]. Other groups have identified peptidomimetic inhibitors of the *H. pylori* T4SS, but the targets of these molecules are not known[26]. Certain unsaturated fatty acids inhibit bacterial conjugation and the ATPase activity of the VirB11 homolog TrwD from plasmid R388, but there is no high-resolution structural information available on their binding site[27–29]. High-throughput small molecule screening and chemical synthesis led to the identification of inhibitors of the ATPase activity of Cagα that likely bind at the ATPase active site, but structural information on their binding site is not available[30,31]. Whereas the isolation of competitive inhibitors of the ATPase activity of VirB11 homologs is interesting, there are concerns about the specificity of these molecules since they may also inhibit other ATPases in bacteria or in mammalian cells.

To identify novel chemical entities that inhibit Cagα we here present an unbiased approach that does not specifically target its ATPase activity. To this effect, we carried out fragment based-screening using differential scanning fluorimetry (DSF) to identify molecules that bind and stabilize Cagα[32]. Four of the molecules inhibit the Cagα ATPase activity and the most potent molecule impacts the conformation of the protein, dissociates the hexamer and it inhibits the production of interleukin-8 upon interaction between *H. pylori* and mammalian cells.

## Results and Discussion

VirB11 like proteins (Cagα in *Helicobacter pylori*) are key components of the T4SS and play a crucial role in energizing the T4SS for substrate secretion. To identify novel chemical entities against Cagα, we have developed a fragment-based screening approach to identify candidate binders, including molecules that may inhibit protein-protein interactions. We have previously used this approach to identify inhibitors of the VirB8 homolog TraE from the plasmid pKM101 conjugation system. We identified molecules that target a known inhibitor binding site on VirB8-like proteins, and we also identified a new binding site showing the potential for the discovery of bioactive molecules and of novel inhibitor target sites[23,24,33].

### Differential scanning fluorimetry to identify Cagα-binding fragments.
We conducted a fragment-based screening approach by using a DSF assay. This assay measures binding of molecules to proteins by changes of the thermal melting profile in the presence of the fluorescent dye Sypro Orange[32]. We validated this assay by testing binding to previously characterized ligands that influence the conformation of Cagα, such as $MgCl_2$, ADP and the non-hydrolysable substrate analog ATP-γ-S. Addition of the nucleotide ligand $MgCl_2$ increases the melting temperature from 37 °C to 42 °C, but in the presence of $MgCl_2$ and ADP or ATP-γ-S, strong increases of the melting temperature to 55 °C and 60 °C were observed, respectively (Fig. 1). The optimized assay conditions were used to screen a library of 505 fragments[24,34] (Supplementary Fig. 1). 16 molecules (Supplementary Fig. 2) were identified that reproducibly increase the melting temperature of Cagα by 1 °C to 4 °C, which is the typical range observed for binding fragments (Supplementary Fig. 1). Interestingly, incubation of many of these fragments in the presence of $MgCl_2$ and ADP reduces the melting temperature when compared to $MgCl_2$ and ADP alone, suggesting that they impact the conformation of Cagα in a way that changes binding of the other ligands (Supplementary Fig. 3). We also identified several molecules that reduce the melting temperature, but those were generally hydrophobic and their addition led to precipitation of Cagα. Since we are interested in molecules that interfere with protein-protein interactions we did not follow up on those that reduce the melting temperature.

### Effects of binding fragments on the Cagα ATPase activity.
We used a Malachite green assay to measure the release of inorganic phosphate from ATP to assess whether the 16 binding fragments impact the enzymatic activity of Cagα. Four of the molecules reduce the ATPase activity and the $IC_{50}$ values range between 196.2 μM for molecule 1G2 (Fig. 2a) and 4.77 mM in case of molecule 2A5 (Table 1 and Supplementary Fig. 4). We used the most potent molecule 1G2 as starting point for a limited structure-activity relationship analysis using six commercially available analogs (Table 1). Two of these molecules (1G2#5 and 1G2#6) do not inhibit the ATPase activity, three of them have higher $IC_{50}$ values than 1G2 (1G2#1, #2 and #3), but molecule 1G2#4 has a lower $IC_{50}$ value of 81.9 μM (Table 1, Fig. 2b and Supplementary Fig. 5). Finally, we tested the mechanism of inhibition by varying the inhibitor concentrations (0 to 500 μM) and the ATP concentrations (0 to 80 μM) and fitting of the initial velocity data using nonlinear regression shows that only the $V_{max}$ was affected, whereas the $K_m$-values remain constant (Fig. 2c,d). Therefore, the mechanism of inhibition by molecules 1G2 and 1G2#4 is non-competitive. These results suggest that we have identified molecules that inhibit the Cagα ATPase activity indirectly via a novel allosteric mechanism.
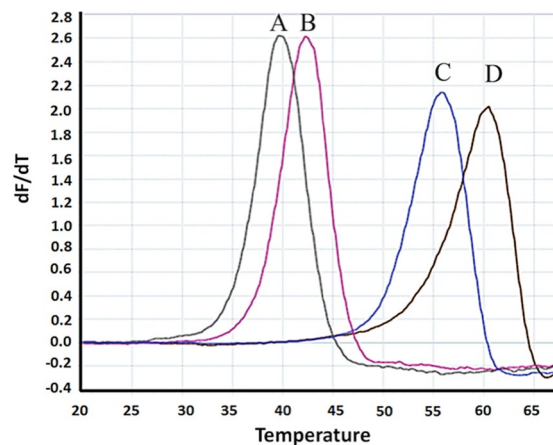
**Figure 1.** Melting temperature of Cagα in the presence of ligands and cofactors. Melting curves for Cagα were determined using differential scanning fluorimetry (DSF). (A) Cagα apoprotein (green, $T_m = 37\,°C$), (B) Cagα and metal cofactor $MgCl_2$ (pink, $T_m = 42\,°C$), (C) Cagα with $MgCl_2$ and ADP (blue, $T_m = 56\,°C$) and (D) Cagα with $MgCl_2$ and ATP-γ-S (black, $T_m = 60\,°C$).
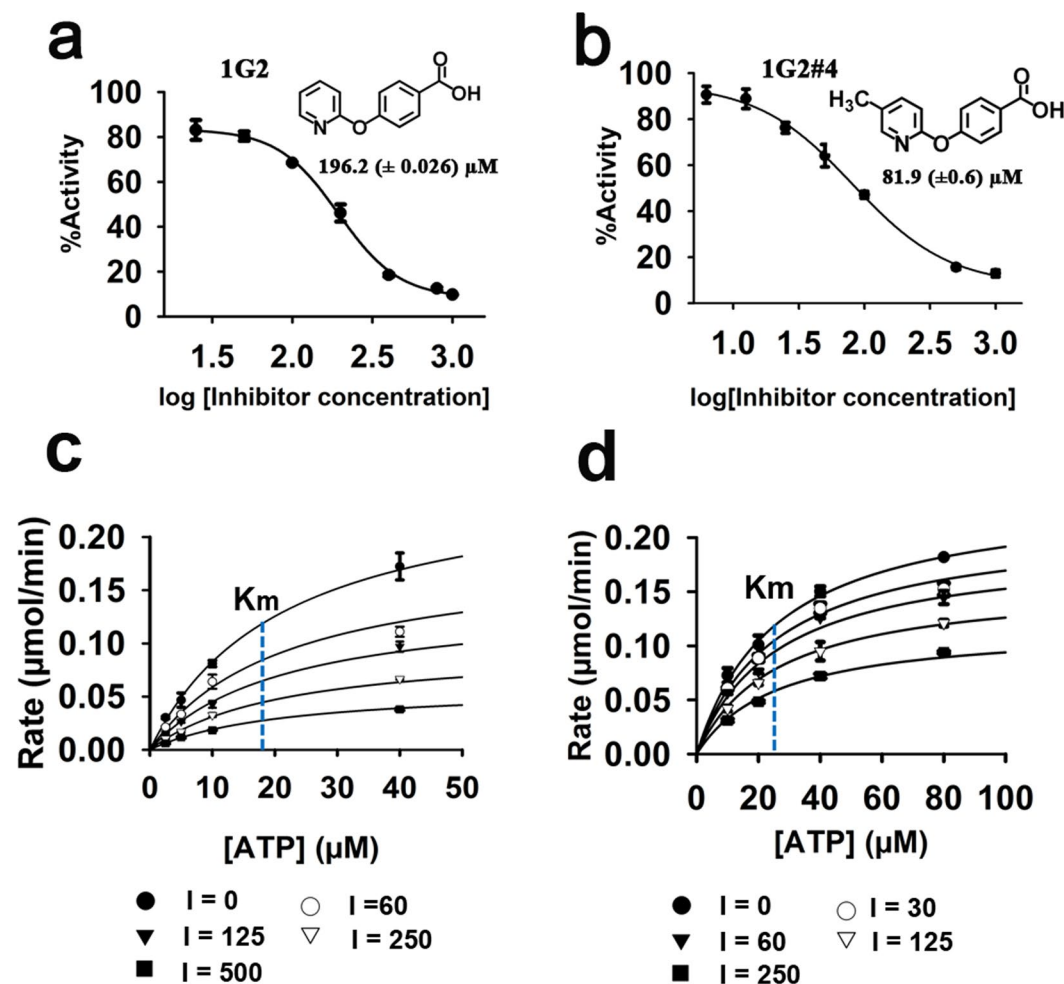


**Figure 2.** Enzyme Kinetics of Cagα in the presence of molecule 1G2 and 1G2#4. (**a,b**) Dose response curves of ATPase activity showing $IC_{50}$ values in the presence of 1G2 and its derivative 1G2#4. (**c,d**) Plot of Cagα ATPase activity versus ATP concentration in the presence of 1G2 and 1G2#4. The data were globally fit to a model of non-competitive inhibition. Concentrations varied from 0 to 500 μM of inhibitors in the presence of 2 mM of $MgCl_2$. The blue lines in (c) and (d) represent $K_m$, which remains constant throughout different inhibitor concentrations.
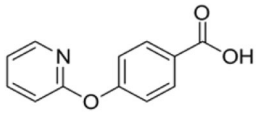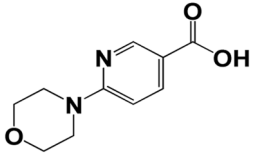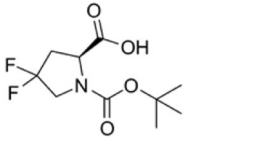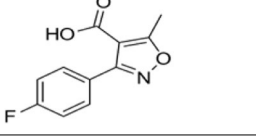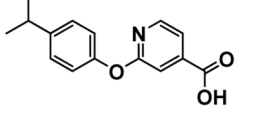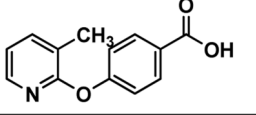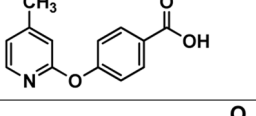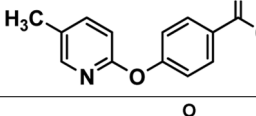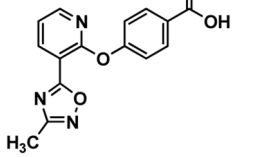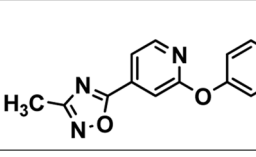
| Name | Structure | IC$_{50}$ values |
|------|-----------|------------------|
| 1G2 | | 196.2 ($\pm$0.026) µM |
| 1G6 | | 0.987 ($\pm$0.076) mM |
| 2A5 | | 4.77 ($\pm$0.053) mM |
| 1F12 | | 1.85($\pm$0.068) mM |
| 1G2#1 | | 547.4 ($\pm$0.59) µM |
| 1G2#2 | | 619.6 ($\pm$0.95) µM |
| 1G2#3 | | 479.6 ($\pm$0.46) µM |
| 1G2#4 | | 81.9 ($\pm$0.6) µM |
| 1G2#5 | | No Inhibition |
| 1G2#6 | | No Inhibition |

**Table 1.** Structures and IC$_{50}$ of molecules that inhibit the ATPase activity of Cagα.

**Binding fragments impact the conformation and dissociate the Cagα hexamer.**    Binding of fragments may impact the conformation and the homo-multimerization of Cagα and we used the homo-bifunctional cross-linking agent disuccinimidyl-suberate (DSS) to obtain insights into the multimerization of the protein. As expected, incubation of Cagα with increasing concentrations of DSS (0–20 µM), followed by SDS-PAGE and western blot analysis, leads to the successive formation of higher molecular mass forms, which is consistent with the formation of a hexamer (Fig. 3a). The cross-linking pattern is similar in the presence of MgCl$_2$ (Fig. 3b), increased amounts of higher molecular mass products are observed in the presence of ADP/MgCl$_2$ (Fig. 3c), but in the presence of ATP-γ-S/MgCl$_2$ (Fig. 3d), and of molecule 1G2 (Fig. 3e) a reduced amount of higher molecular mass complexes is observed. Crosslinking assays provide primarily qualitative information and the data suggest significant changes of the conformation and/or multimerization of Cagα in the presence of ATP-γ-S and 1G2.
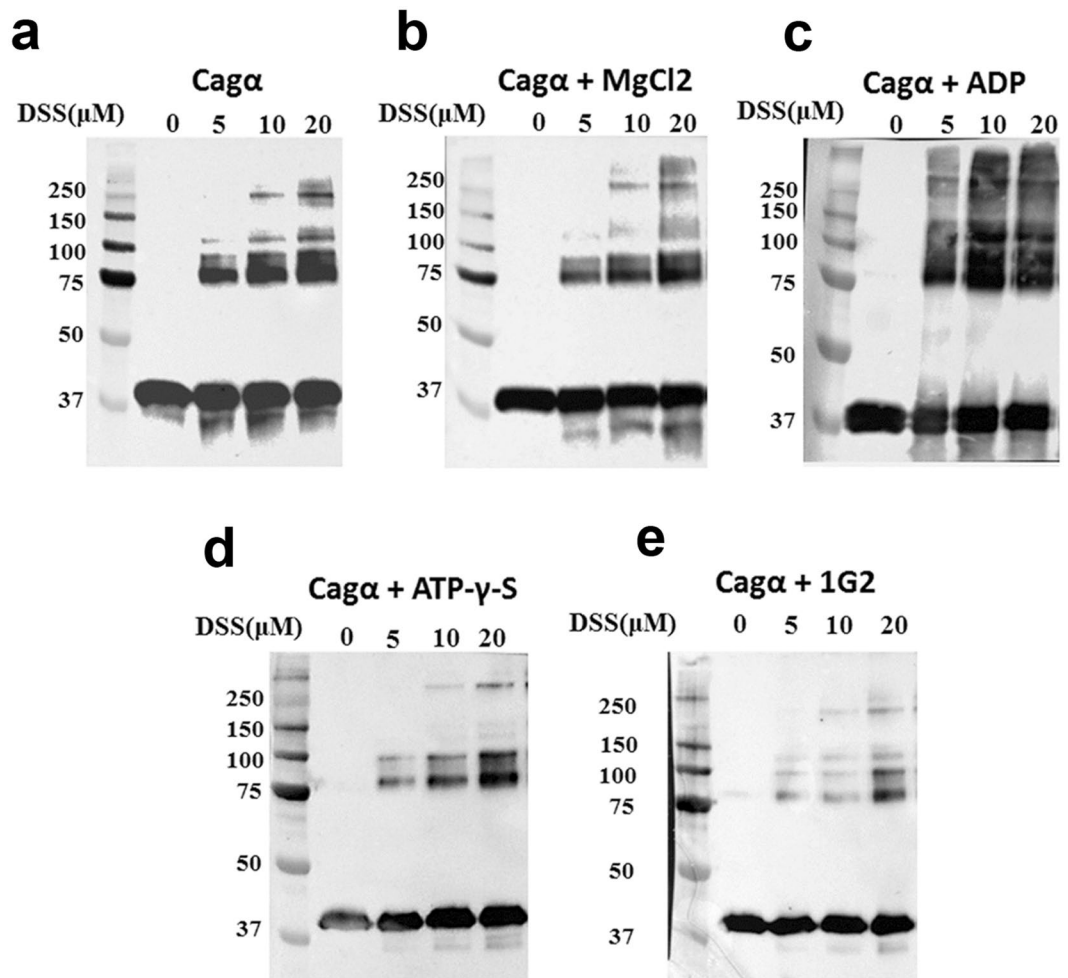
**Figure 3.** Chemical cross-linking using DSS to study the formation of Cagα oligomers in the presence of ligands. (**a**) Cagα apo protein; (**b**) Cagα with $MgCl_2$; (**c**) Cagα with ADP and $MgCl_2$; (**d**) Cagα with ATP-γ-S and $MgCl_2$; (**e**) Cagα with 1G2 and $MgCl_2$. The concentrations of DSS varied between 0 and 50 μM leading to formation of oligomers (indicated by arrows), detection by SDS-PAGE and western blotting using His-tag specific antibodies. Original blots are provided as supplementary dataset.

Next, we performed gel filtration and EM analysis to provide more detailed insights into the effects of 1G2 on protein conformation. After gel filtration, Cagα protein homogeneously elutes as a single peak with an elution volume corresponding to a molecular mass of 244 kDa, which is consistent with the formation of a hexamer (Fig. 4). The same elution volume is observed in the presence of ATP-γ-S. Interestingly, when Cagα was pre-incubated with molecule 1G2 we observe the elution of two peaks (peak A and peak B in Fig. 4) with elution volumes corresponding to apparent molecular masses of 175 kDa and 54 kDa, respectively. These results suggest that incubation with molecule 1G2 dissociates the Cagα hexamer into lower molecular mass species. Analysis by negative staining electron microscopy reveals hexamers in the absence of 1G2 (Fig. 5a, inset shows a particle of 12 nm diameter). After addition of 1G2 we observe some large rings and different types of lower molecular mass species in peak A (Fig. 5b, inset shows one type of particle of 7 nm diameter that may be a tetramer). We observe exclusively lower mass species in the presence of 1G2 in peak B (Fig. 5c) that probably represent monomeric Cagα. Therefore, gel filtration and EM analysis revealed that binding to 1G2 successively dissociates the Cagα-hexamer. Previously described Cagα inhibitors were believed to bind to the active site and the known competitive inhibitor ATP-γ-S does not dissociate the hexamer. The mechanism of inhibition identified here is therefore novel and it would be interesting to assess the molecular basis of dissociation using X-ray crystallography or approaches that are more sensitive to conformational changes such as analytical ultracentrifugation, dynamic light scattering or high-resolution cryo-electron microscopy.

**Molecule 1G2 inhibits the production of interleukin-8 upon binding of *H. pylori* to AGS cells.** Finally, we assessed whether molecule 1G2 or its derivates impact the functionality of the T4SS *in vivo*. To this effect, we tested their impact on the interaction of *H. pylori* strain 26695 with gastric adenocarcinoma (AGS) cells. First, we tested their toxicity and found that molecule 1G2 and derivates 1G2#1 to #6 have no negative effect on the growth of *H. pylori* on solid agar media at concentrations up to 500 μM (Supplementary Fig. 6). Similarly, most molecules do not have negative impact on the viability of AGS cells at concentrations up to 500 μM, showing
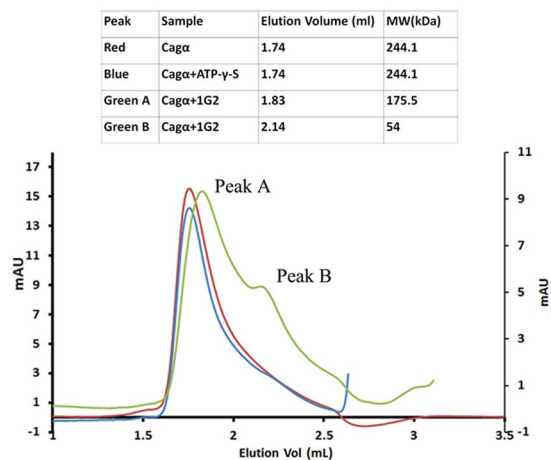
| Peak | Sample | Elution Volume (ml) | MW(kDa) |
|---|---|---|---|
| Red | Cagα | 1.74 | 244.1 |
| Blue | Cagα+ATP-γ-S | 1.74 | 244.1 |
| Green A | Cagα+1G2 | 1.83 | 175.5 |
| Green B | Cagα+1G2 | 2.14 | 54 |



**Figure 4.** Analytical size exclusion chromatography of Cagα apoprotein and in the presence of ligands. Proteins were separated by gel filtration over a Superdex 200 column. Cagα apoprotein elutes as a hexamer (red curve), elution of Cagα-ATP-γ-S (blue curve) and of two lower molecular mass peaks (A and B) after incubation of Cagα with 1G2 (in green). The molecular masses characterized according to the elution volume are summarized in the table above the graph.
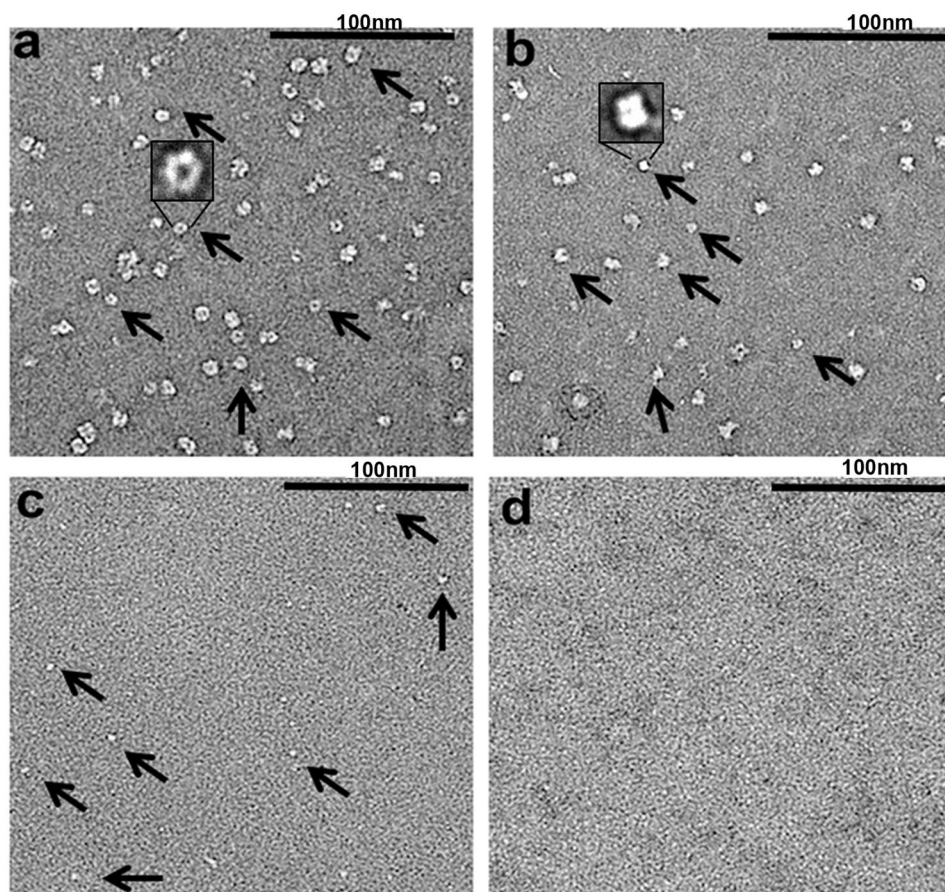


**Figure 5.** Electron micrographs of negatively stained Cagα apoprotein after gel filtration. Analysis by transmission electron microscopy and negative staining of (**a**) Cagα apoprotein shows a hexameric ring-like structure, insert shows a typical particle; (**b**) peak A of Cagα incubated with 1G2 after elution from the gel-filtration, inset shows a typical smaller particle, but the sample is heterogeneous and (**c**) peak B, probably representing monomeric Cagα. (**d**) Negative control grid. Arrows show the differently sized complexes and size bars indicate the dimensions.
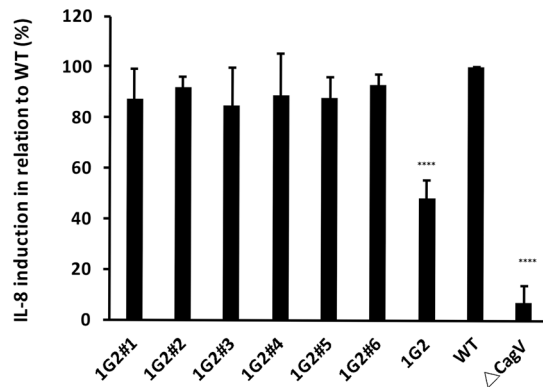
**Figure 6.** Molecule 1G2 decreases IL-8 induction in co-cultivated AGS cells. *H. pylori* 26695 without and after pre-incubation with 1G2 and its derivatives for 40 min. AGS cells were then co-cultured with *H. pylori* overnight and IL-8 induction was measured by ELISA. The induction of IL-8 by the wild type was calculated as 100% (WT), induction of IL-8 by the *ΔcagV* strain was used as negative control. The data represent the results from three experiments.

that they are not toxic (Supplementary Fig. 7). We then tested the effects of these molecules in two commonly used assays for downstream effects of T4SS function: IL-8 production and CagA phosphorylation. When we test the effects of these molecules at 200 μM concentration on the production of IL-8 by AGS cells upon co-cultivation with *H. pylori*, 1G2 significantly reduces the production of this proinflammatory cytokinine to about 50% of the control (Fig. 6). In contrast, derivates 1G2#1 to #6 have no effect on IL-8 production. Similarly, none of the molecules reduces the tyrosine phosphorylation of the T4SS-translocated virulence factor CagA, which is generally used as an alternative assay to measure T4SS function (Supplementary Fig. 8). It was somewhat unexpected that molecule 1G2 inhibited IL-8 production to 50% of the control values, but we did not observe an effect on CagA phosphorylation. This observation may be due to partial inhibition of T4SS function by 1G2 that is more readily quantifiable in the IL-8 production assay as compared to the CagA phosphorylation assay. Molecule 1G2#4 had a stronger inhibitory effect on Cagα enzyme activity *in vitro* than 1G2, but this molecule had no effect in the *in vivo* assays, which may be due to its higher hydrophobicity impacting solubility and penetration into cells.

In conclusion, we have here analyzed six derivatives of molecule 1G2 that were commercially available and in future work we will conduct a more exhaustive structure-activity relationship analysis to synthesize more potent molecules. Potent inhibitors of Cagα could be developed into anti-virulence drugs that are alternative or complementary treatments to currently used triple or quadruple therapy. It would also be interesting to test the specificity of these molecules to assess whether they are narrow or broad-spectrum inhibitors that also impact other T4SS, e.g. bacterial conjugation systems[28,35].

## Methods

**Bacterial strains, cell lines and culture conditions.** *H. pylori* strains 26695 and *ΔcagV* (*hp0530*) mutant have been described[36] and were cultivated on Columbia agar base (BD) containing 10% (v/v) defibrinated horse blood (Wisent Inc.), vancomycin (10 μg/ml) and amphotericin B (10 μg/ml). Chloramphenicol (34 μg/ml) was added in case of the *ΔcagV* strain to select for the *cam* gene cassette used to disrupt the gene. For liquid culture, brain heart infusion (BHI) media (Oxoid) were supplemented with 8% fetal bovine serum (FBS) and appropriate antibiotics. Bacteria were cultivated at 37 °C, under microaerophilic conditions (5% oxygen, 10% $CO_2$). AGS cells were grown at 37 °C in F12K media (Wisent Inc.) with 10% (v/v) FBS (Wisent Inc.) in a 5% $CO_2$ containing atmosphere.

**Cloning, expression and purification of Cagα.** The Cagα encoding gene from *H. pylori* 26695 (ATCC) was PCR-amplified from genomic DNA with primers (forward, 5′-TAGCGAATTCGGTACCATGACTGAAGA CAGATTGAGTGCA-3′ and reverse, 5′-CGATGAATTCCTCGAGCTACCTGTGTGTTTGATATAAAATTC-3′). The PCR product was ligated in between restriction enzymes *Nhe*I and *Xho*I, into expression vector pET28a. Expression was conducted in *E. coli* BL21 (DE3) cultivated in two liters of LB-medium at 37 °C at 220 rpm, protein production was induced at $OD_{600}$ of 1.0 with 1 mM isopropylthio-β-galactoside (IPTG), followed by further incubation for 16 h at 25 °C. For purification, the cell pellet was suspended in binding buffer (50 mM HEPES, 500 mM NaCl, 20 mM imidazole, pH 7.5, 10% glycerol, 0.1% triton, plus two tablets of EDTA-free protease inhibitor cocktail (Roche)) and lysed using a cell disrupter (Constant Systems Inc.) at 27 kPsi, followed by centrifugation at 15,000 rpm at 4 °C to reduce cell debris. The supernatant was loaded onto a His-trap Ni-NTA column (GE Healthcare), and eluted using a linear 50 ml gradient of 40–500 mM imidazole in binding buffer. Proteins were then dialysed (25 mM sodium phosphate, 125 mM NaCl, 5 mM DTT, pH 7.4) and subjected to Size exclusion chromatography using a Superdex-200 column (GE Healthcare) with buffer 25 mM HEPES pH7.5 and 100 mM NaCl and peak fractions were analyzed by SDS-PAGE. The fractions containing Cagα hexamers were pooled and concentrated to 6 mg/ml for crystallographic studies.

**Analytical gel filtration chromatography.** Purified protein was further characterized by analytical gel filtration (Superdex 200) in 25 mM HEPES, pH 7.5 and 50 mM NaCl (pH 7.5). The column volume was 3 ml and the protein was injected at a flow rate of 0.5 ml/min. To study the effects of ATP-γ-S and of 1G2, 35 μg of Cagα was pre-incubated with 2 mM of the molecules for 30 min, followed by analytical size exclusion analysis.

**Enzyme activity assay.** The ATPase activity was quantified using a malachite green binding assay[37]. The 100 μL reaction mixtures contained 25 mM HEPES (pH 7.5), 100 mM NaCl, 60 nM of enzyme and 200 μM of MgCl₂ with different concentrations of ATP (0 μM–320 μM) to determine kinetic parameters. The reaction mixtures were incubated for 30 min at 30 °C and then 40 μL of malachite green assay mixture was added. The formation of the blue phosphomolybdate-malachite green complex was in linear relation to the amount of released inorganic phosphate and measured at 610 nm. To study the mechanism of inhibition, the concentrations of inhibitors were varied between 0 and 500 μM with different concentrations of ATP (0–40 μM). Initial velocity data were fit using nonlinear regression analysis to each of the equations describing partial and full models of competitive, uncompetitive, non-competitive, and mixed inhibition using the Enzyme Kinetics Module of SigmaPlot (SigmaPlot version 11.0 software). On the basis of the analysis of fits through "goodness-of-fit" statistics, the full non-competitive inhibition model was determined with the equation $\nu = V_{max}/[(1 + [I]/K_i) \times (1 + K_m/[S])]$, where $[S] = [ATP]$, $[I] = [1G2]$.

**IC₅₀ determination.** IC₅₀ values were determined by incubating different concentrations of molecules (10–1,000 μM; from stocks of 200 mM) with enzyme in 25 mM HEPES (pH 7.5) and 100 mM NaCl. Mixtures were incubated with inhibitors for 15 min, followed by addition of ATP and incubation for 30 min at 37 °C. The reactions were stopped by addition of 40 μl malachite green solution and the inorganic phosphate released was determined at 610 nm. Data were plotted as 1/rate versus inhibitor concentration for each substrate concentration and a linear fit was calculated by non-linear regression using SigmaPlot (version 11.0).

**Differential scanning fluorimetry (DSF).** A fragment library of 505 molecules was used as in our previous work[34]. The reaction mixture contains 5 μM of Cagα, 10x concentration of SYPRO Orange (from 5000x stock solution (ThermoFisher)) in 50 mM HEPES (pH 7.5), 100 mM NaCl and 5% final concentration of DMSO. The fragments and nucleotides were added to final concentrations of 5 mM, and the fluorescence was monitored over 20–95 °C with a LightCycler 480 instrument (Roche).

**Analysis of protein-protein interactions by cross-linking.** Chemical cross-linking with disuccinimidyl suberate (DSS; Pierce) was performed as described[38]. 100 nM of Cagα in 50 mM HEPES (pH 7.5) and 100 mM NaCl were first incubated with cofactors (MgCl₂, ADP) or inhibitors (ATP-γ-S, 1G2) for 30 min, followed by crosslinking with DSS (0–50 μM) for 1 h, and reactions were stopped by mixing with an equal volume of 2 × Laemmli buffer. The formation of cross-linking products was analyzed by SDS-PAGE and western blotting using His-tag specific antiserum and ImageLab 4.0 software (Bio-Rad).

**Electron microscopy and image processing.** Carbon-coated grids were negatively glow-discharged at 15 mA and 0.4 mBar for 30 sec. 5 μl of purified protein at a concentration of 2 ng/μl was spotted onto the grids for 60 sec and blotted using grade 1 Whatman filter paper, followed by staining with freshly prepared 1.5% uranyl formate solution for 60 sec and drying. The samples were imaged at a magnification of 49,000-fold (pixel size: 2.2 Å/pixel) with a defocus of −2.5 μm using a FEI Tecnai T12 electron microscope (FEMR facility at McGill University). Transmission Electron Microscope (TEM) equipped with a Tungsten filament and operated at 120 kV equipped with a 4k × 4k CCD camera (Gatan Ultrascan 4000 CCD camera system model 895). Subsequently, the images were processed using ImageJ.

**Measurement of *H. pylori* and AGS cell viability.** AGS cell viability was monitored using Cell Proliferation Reagent WST-1 (Sigma). To evaluate the sensitivity of *H. pylori* to 1G2 and its derivates, freshly harvested bacteria were spread on a 150-mm agar plate. Increasing concentrations of compounds (50–500 μM) were spotted onto Whatman paper disks and growth was observed after 72 h incubation at 37 °C under microaerophilic conditions and compared to antibiotics (50–250 μM).

**Assay for monitoring CagA transfer into AGS cells.** Preceding the infection, an overnight culture of *H. pylori* was pre-incubated with 1G2 and its derivates for 30 min. AGS cells at 6 × 10⁵ cells/well density in 6-well plates were infected with the pre-treated cultures of *H. pylori* for 3–6 h at a multiplicity of infection of 100:1. Cells were washed twice with PBS, harvested and lysed at 4 °C in RIPA buffer (150 mM NaCl, 50 mM Tris/HCl, pH 8, 1% NP-40, 2 mM Na₃VO₄, supplemented with Complete Protease Inhibitor Tablet (Roche). After 15 min of centrifugation at 16,000 g, lysates were separated by SDS-PAGE, followed by western blotting with mouse polyclonal antiserum raised against CagA (Abcam), anti-phosphotyrosine (PY99; Santa Cruz Biotechnology) and anti-β-actin (C4, Santa Cruz Biotechnology).

**Assay for IL-8 induction.** Preceding the infection, an overnight culture of *H. pylori* was pre-incubated with 1G2 and its derivates for 30 min. AGS cells at 6 × 10⁵ cells/well density in 6-well plates were infected with the pre-treated cultures of *H. pylori* at a multiplicity of infection of 100:1. After 24 h incubation under microaerophilic conditions, supernatants were sampled and centrifuged (15,000 g), before freezing at −80 °C. The level of IL-8 in cell culture supernatants was determined by using a commercially available human IL-8 ELISA kit (Invitrogen).

### Data Availability
Materials, data and associated protocols will be made available on request.

# References

1. Malfertheiner, P., Link, A. & Selgrad, M. Helicobacter pylori: perspectives and time trends. *Nature reviews. Gastroenterology & hepatology* **11**(10), 628–638 (2014).
2. Herrero, R., Parsonnet, J. & Greenberg, E. R. Prevention of gastric cancer. *Jama* **312**(12), 1197–8 (2014).
3. Plummer, M., Franceschi, S., Vignat, J., Forman, D. & de Martel, C. Global burden of gastric cancer attributable to Helicobacter pylori. *International journal of cancer. Journal international du cancer* **136**(2), 487–90 (2015).
4. Gatta, L., Vakil, N., Vaira, D. & Scarpignato, C. Global eradication rates for Helicobacter pylori infection: systematic review and meta-analysis of sequential therapy. *Bmj* **347**, f4587 (2013).
5. Ochman, H., Lawrence, J. G. & Groisman, E. A. Lateral gene transfer and the nature of bacterial innovation. *Nature* **405**(6784), 299–304 (2000).
6. Grohmann, E., Christie, P. J., Waksman, G. & Backert, S. Type IV secretion in Gram-negative and Gram-positive bacteria. *Molecular microbiology* **107**(4), 455–471 (2018).
7. Segal, E. D., Cha, J., Lo, J., Falkow, S. & Tompkins, L. S. Altered states: involvement of phosphorylated CagA in the induction of host cellular growth changes by Helicobacter pylori. *Proc Natl Acad Sci USA* **96**(25), 14559–64 (1999).
8. Backert, S. *et al.* Translocation of the Helicobacter pylori CagA protein in gastric epithelial cells by a type IV secretion apparatus. *Cellular microbiology* **2**(2), 155–64 (2000).
9. Fischer, W. *et al.* Systematic mutagenesis of the *Helicobacter pylori cag* pathogenicity island: essential genes for CagA translocation in host cells and induction of interleukin-8. *Mol. Microbiol.* **42**, 1337–1348 (2001).
10. Selbach, M., Moese, S., Meyer, T. F. & Backert, S. Functional analysis of the *Helicobacter pylori* cag pathogenicity island reveals both VirD4-CagA-dependent and VirD4-CagA-independent mechanisms. *Infect. Immun.* **70**, 665–671 (2002).
11. Tegtmeyer, N., Neddermann, M., Asche, C. I. & Backert, S. Subversion of host kinases: a key network in cellular signaling hijacked by Helicobacter pylori CagA. *Molecular microbiology* **105**(3), 358–372 (2017).
12. Naumann, M., Sokolova, O., Tegtmeyer, N. & Backert, S. Helicobacter pylori: A Paradigm Pathogen for Subverting Host Cell Signal Transmission. *Trends Microbiol* **25**(4), 316–328 (2017).
13. Gall, A., Gaudet, R. G., Gray-Owen, S. D. & Salama, N. R. TIFA Signaling in Gastric Epithelial Cells Initiates the cag Type 4 Secretion System-Dependent Innate Immune Response to Helicobacter pylori Infection. *Mbio*, **8**(4) (2017).
14. Krause, S. *et al.* Sequence-related protein export NTPases encoded by the conjugative transfer region of RP4 and by the cag pathogenicity island of Helicobacter pylori share similar hexameric ring structures. *Proc Natl Acad Sci USA* **97**(7), 3067–72 (2000).
15. Krause, S., Pansegrau, W., Lurz, R., de la Cruz, F. & Lanka, E. Enzymology of type IV macromolecule secretion systems: the conjugative transfer regions of plasmids RP4 and R388 and the cag pathogenicity island of Helicobacter pylori encode structurally and functionally related nucleoside triphosphate hydrolases. *J Bacteriol* **182**(10), 2761–70 (2000).
16. Savvides, S. N. *et al.* VirB11 ATPases are dynamic hexameric assemblies: new insights into bacterial type IV secretion. *EMBO J.* **22**, 1969–1980 (2003).
17. Yeo, H. J., Savvides, S. N., Herr, A. B., Lanka, E. & Waksman, G. Crystal structure of the hexameric traffic ATPase of the *Helicobacter pylori* type IV secretion system. *Mol. Cell* **6**, 1461–1472 (2000).
18. Fujita, Y. *et al.* Hakai, a c-Cbl-like protein, ubiquitinates and induces endocytosis of the E-cadherin complex. *Nat Cell Biol* **4**(3), 222–31 (2002).
19. Hare, S., Bayliss, R., Baron, C. & Waksman, G. A large domain swap in the VirB11 ATPase of Brucella suis leaves the hexameric assembly intact. *Journal of molecular biology* **360**(1), 56–66 (2006).
20. Brown, E. D. & Wright, G. D. Antibacterial drug discovery in the resistance era. *Nature* **529**(7586), 336–43 (2016).
21. Ruer, S., Pinotsis, N., Steadman, D., Waksman, G. & Remaut, H. Virulence-targeted Antibacterials: Concept, Promise, and Susceptibility to Resistance Mechanisms. *Chem Biol Drug Des* **86**(4), 379–99 (2015).
22. Paschos, A. *et al.* An *In Vivo* High-Throughput Screening Approach Targeting the Type IV Secretion System Component VirB8 Identified Inhibitors of Brucella abortus 2308 Proliferation. *Infect Immun* **79**(3), 1033–43 (2011).
23. Smith, M. A. *et al.* Identification of the Binding Site of Brucella VirB8 Interaction Inhibitors. *Chem Biol* **19**(8), 1041–8 (2012).
24. Casu, B., Arya, T., Bessette, B. & Baron, C. Fragment-based screening identifies novel targets for inhibitors of conjugative transfer of antimicrobial resistance by plasmid pKM101. *Sci Rep* **7**(1), 14907 (2017).
25. Casu, B. *et al.* Structural analysis and inhibition of TraE from the pKM101 type IV secretion system. *J Biol. Chem.* **291**, 23817–23829 (2016).
26. Shaffer, C. L. *et al.* Peptidomimetic Small Molecules Disrupt Type IV Secretion System Activity in Diverse Bacterial Pathogens. *MBio* **7**(2), e00221–16 (2016).
27. Ripoll-Rozada, J. *et al.* Type IV traffic ATPase TrwD as molecular target to inhibit bacterial conjugation. *Molecular microbiology* **100**(5), 912–21 (2016).
28. Cabezon, E., de la Cruz, F. & Arechaga, I. Conjugation Inhibitors and Their Potential Use to Prevent Dissemination of Antibiotic Resistance Genes in Bacteria. *Front Microbiol* **8**, 2329 (2017).
29. Garcia-Cazorla, Y. *et al.* Conjugation inhibitors compete with palmitic acid for binding to the conjugative traffic ATPase TrwD, providing a mechanism to inhibit bacterial conjugation. *The Journal of biological chemistry* (2018).
30. Hilleringmann, M. *et al.* Inhibitors of Helicobacter pylori ATPase Cagalpha block CagA transport and cag virulence. *Microbiology* **152**(Pt 10), 2919–30 (2006).
31. Sayer, J. R. *et al.* 2- and 3-substituted imidazo[1,2-a]pyrazines as inhibitors of bacterial type IV secretion. *Bioorg Med Chem* **22**(22), 6459–70 (2014).
32. Mashalidis, E. H., Sledz, P., Lang, S. & Abell, C. A three-stage biophysical screening cascade for fragment-based drug discovery. *Nature protocols* **8**(11), 2309–24 (2013).
33. Casu, B. *et al.* VirB8 homolog TraE from plasmid pKM101 forms a hexameric ring structure and interacts with the VirB6 homolog TraD. *Proceedings of the National Academy of Sciences of the United States of America* **115**, 5950–5955 (2018).
34. Sharifahmadian, M. *et al.* Monomer-to-dimer transition of Brucella suis type IV secretion system component VirB8 induces conformational changes. *The FEBS journal* **284**(8), 1218–1232 (2017).
35. Zambelloni, R., Marquez, R. & Roe, A. J. Development of antivirulence compounds: a biochemical review. *Chem Biol Drug Des* **85**(1), 43–55 (2015).
36. Fischer, W. *et al.* Systematic mutagenesis of the Helicobacter pylori cag pathogenicity island: essential genes for CagA translocation in host cells and induction of interleukin-8. *Mol Microbiol* **42**(5), 1337–48 (2001).
37. Cogan, E. B., Birrell, G. B. & Griffith, O. H. A robotics-based automated assay for inorganic and organic phosphates. *Anal Biochem* **271**(1), 29–35 (1999).
38. Yuan, Q. *et al.* Identification of the VirB4-VirB8-VirB5-VirB2 pilus assembly sequence of type IV secretion systems. *J Biol Chem* **280**(28), 26349–59 (2005).

# Acknowledgements

## Author Contributions

T.A. conducted experiments, analyzed data and wrote manuscript. F.O. conducted experiments, analyzed data and wrote manuscript. B.C. conducted experiments, analyzed data. B.B. conducted experiments, analyzed data. J.S analyzed data. C.B. analyzed data and wrote manuscript.

## Additional Information

**Supplementary information** accompanies this paper at https://doi.org/10.1038/s41598-019-42876-6.

**Competing Interests:** The authors declare no competing interests.

**Publisher's note:** Springer Nature remains neutral with regard to jurisdictional claims in published maps and institutional affiliations.